Disease Markers 19 (2003,2004) 107–121
IOS Press

Near-infrared fluorescence optical imaging and tomography

Michael Gurfinkel[a,d], Shi Ke[c], Xiaoxia Wen[c], Chun Li[c,*] and Eva M. Sevick-Muraca[a,b,d,*]
[a]*Department of Chemical Engineering, Texas A&M University, College Station, TX 77843-3122, USA*
[b]*Department of Chemistry, Texas A&M University, College Station, TX 77842-3012, USA*
[c]*Department of Diagnostic Radiology, The University of Texas M.D. Anderson Cancer Center, Houston, TX 77030, USA*
[d]*The Photon Migration Laboratories, Texas A&M University, College Station, TX 77843-3573, USA*

Abstract. The advent of recent advances in near-infrared laser diodes and fast electro-optic detection has spawned a new research field of diagnostic spectroscopy and imaging based on targeting and reporting exogenous fluorescent agents. This review seeks to concisely address the physics, instrumentation, advancements in tomography, and near-infrared fluorescent contrast agent development that promises selective and specific molecular targeting of diseased tissues. As an example of one area of the field, recent work focusing on pharmacokinetic analysis of fluorophores targeting the epidermal growth factor receptor (EGFR) is presented in a human breast cancer xenograft mouse model to demonstrate specificity of molecularly targeted contrast agents. Finally, a critical evaluation of the limitations and the opportunities for future translation of fluorescence-enhanced optical imaging of deep tissues is presented.

1. Introduction: Fluorescence-enhanced optical imaging

Near-infrared (NIR) light of 700–900 nm can penetrate several centimeters of tissue without the harmful radiation effects of gamma rays, x-rays, or ultraviolet light. As a result, over the past several years considerable interest has been focused on the integration of optics and medicine, principally on the development of clinically relevant diagnostic imaging techniques. Because of the low absorbance of endogenous chromophores such as oxy- and deoxyhemoglobin, melanin, and fat, NIR light can propagate significant distances via multiple scattering, enabling imaging of deep ($>$ 1 cm) tissues. The ability to detect late-stage breast cancers using tomographic imaging based on the intrinsic contrast provided by hemoglobin absorption as a result of tumor-initiated angiogenesis has been demonstrated [1]. Unfortunately, the necessity of angiogenesis-mediated absorption contrast limits the potential of NIR optical imaging because small lesions possess insufficient vascularity for endogenous optical contrast. Hence, NIR optical techniques can be expanded through the use of exogenous contrast-enhancing agents. Exogenous fluorophores have been shown to provide superior enhanced contrast when time-dependent measurements of light propagation are employed [2,3]. Furthermore, new and future opportunities for molecular-based diagnostic imaging are afforded when optical imaging techniques are coupled with NIR-excitable fluorescent contrast agents developed for *in vivo* targeting and reporting of cancer and other tissue abnormalities.

In this review, we focus upon the measurement approaches, promises for tomography, and advances in fluorescent contrast-agent development that are directed toward molecular targeting of disease. We fur-

*Corresponding authors: E.M. Sevick-Muraca, The Photon Migration Laboratories, TAMU 3573, College Station, TX 77843-3573, USA. Tel.: +1 979 458 3206; Fax: +1 979 458 1011; E-mail: eva-m-sevick@tamu.edu. Chun Li, Department of Experimental Diagnostic Imaging, The University of Texas M.D. Anderson Cancer Center, 1515 Holcombe Blvd. Box 59, Houston, TX 77030-4009, USA. Tel.: +1 713 792 5182; Fax: +1 713 794 5456; E-mail: cli@di.mdacc.tmc.edu.

ISSN 0278-0240/03,04/$17.00

ther demonstrate that the specific binding or uptake of fluorescent agents directly impacts the pharmacokinetics of agent distribution, which can be evaluated readily with NIR imaging techniques. Finally, since NIR-excitable probes provide the promise for deep-tissue localization in clinical applications, we discuss the translation of fluorescent dye development to pertinent diagnostic applications.

1.1. NIR measurement approaches

There are three distinct methods for monitoring the propagation of NIR light and the emission of generated fluorescent light. These methods are continuous wave (CW), time-domain photon migration (TDPM), and frequency-domain photon migration (FDPM). The earliest and simplest methods of measuring NIR light interaction with tissue involve intensity-based or CW techniques. CW techniques generally involve measuring the spatial distribution of light intensity at the tissue surface resulting from illumination by a source of constant intensity. CW techniques may be used to measure NIR fluorescence from exogenous contrast agents with a point or area light source at the excitation wavelength incident on the tissue surface. The collection of the fluorescence re-emitted from the tissue surface occurs through a point or area detector that discriminates the re-emitted fluorescence from the excitation light. Because the excitation light fluence (which represents the amount of light in terms of its local concentration [photons/volume] times the speed of light [length/time], or alternatively in terms of a flux [photons/area/time]) exponentially attenuates as it travels from the tissue surface, the excitation fluence always remains greatest at the tissue surface. Furthermore, the amount of generated fluorescence at any given position within the tissue is proportional to the product of the local fluorophore concentration and the local excitation fluence. As a result, a low concentration of fluorophore at or near the tissue surface can produce the bulk of the detected signal emitted and collected in CW techniques. A consequence of CW methods is that the signal from a deeper embedded target containing a high concentration of fluorophore may be masked easily by a very low concentration of fluorophore at or near the tissue surface. As discussed below, methods that measure the time-dependence of light propagation may escape this limitation.

In addition to measuring the spatial distribution of light intensity, time-dependent measurement approaches also are capable of measuring the temporal distribution of the detected light. Time-resolved techniques employ an excitation light source whose intensity varies with time. TDPM techniques make use of ultra-short (femtosecond-picosecond) light pulses and detectors that either are fast, time-gated, or single-photon counting devices. A light pulse is delivered to the tissue, which, as a result of multiple scattering, broadens with nanosecond "time-of-flight" and attenuates as it propagates through the tissue. In the presence of an NIR-excitable fluorophore, a fluorescence pulse is generated within the tissue that increasingly is broadened and attenuated owing to the fluorescence decay kinetics of the fluorophore. Because the region of highest excitation light fluence is not constant and propagates away from the tissue surface with time, the spatial location of the generated fluorescent pulse also varies, resulting in the deeper origin of fluorescent signals re-emitted at the tissue surface. As a result, as long as the lifetime or the average time for relaxation of the fluorophore is less than or comparable to the "time-of-flight" associated with light propagation, the detected fluorescence may, as a function of time, originate from various depths within the tissue in time-dependent measurement methods [4].

An alternative time-dependent measurement methodology, which is directly related to TDPM through the Fourier transform, is known as FDPM. In this approach, a light source that is sinusoidally intensity-modulated at radio frequencies is used to launch photons into the tissue. Typically, modulation frequencies range from 30–200 MHz. As the intensity-modulated light (also referred to as a "photon density wave") propagates through the tissue, its amplitude is attenuated and it experiences a phase-lag relative to the incident light. In the presence of an NIR fluorophore, the intensity-modulated excitation fluence results in a fluorescent "photon density wave" or intensity-modulated emission fluence that is further amplitude-attenuated and phase-delayed, owing to the fluorescent decay kinetics of the dye in its current environment [5]. The phase-lag and amplitude-attenuation of the detected fluorescent photon density wave, measured relative to the incident light wave using a fast detector or array of detectors, are pronounced owing to the fluorophore's decay kinetics. As a result, fluorescence-enhanced FDPM may be used to exploit the fluorescent relaxation process to improve contrast in the phase-lag and amplitude-attenuation of the detected signal.

Similar to TDPM, the excitation light fluence in FDPM also varies in time and space, and the region of highest excitation fluence is not located consistently at

the tissue surface. Consequently, as long as the product of the fluorophore lifetime and modulation frequency is less than one, the detected fluorescence may originate from deep within the tissue, even in the presence of background dye [6]. Another important feature of FDPM measurements concerns their inherent insensitivity to ambient light. Because the amplitude of the detected fluorescent signal is unaffected by non-modulated ambient light, FDPM enables greater sensitivity and depth of penetration than do conventional CW techniques [7,8].

1.2. NIR fluorescence-enhanced optical imaging

The preponderance of NIR fluorescence imaging studies conducted to date have focused on CW measurements in a rodent model using either an array of point illumination and an array of point collection of generated fluorescence, or area illumination with an expanded excitation beam and collection of the generated fluorescence using an array detector, or a simple charge-coupled device (CCD) camera (for review see reference [8]). The use of a point source of illumination light and point collection of generated fluorescent light is the most inefficient means to image an entire tissue but is advantageous since current tomographic algorithms focus on reconstruction of optical properties in the volume of tissues "sampled" between the incident illumination and collection points on the surface of a tissue (see below). The excitation light that originates from a point on the tissue surface and that ultimately is detected at another point on the tissue surface has sampled a finite volume [9]. The detected fluorescence also is constrained to within this "sampling volume". Consequently, a number of measurements of point illumination/point collection pairs are required to sample the entire tissue, and tomographic reconstruction is required. In contrast, employing an expanded beam to deliver excitation light results in a larger sampling volume and, hence, in fluorescence re-emitted from a greater volume of tissue. When time-dependent measurements are employed, the re-emitted fluorescence may originate from a greater depth from the tissue surface, as described in the earlier section.

Many investigators have employed CW measurements of targeting fluorophores in rodents utilizing whole-animal illumination with an expanded excitation beam and a simple CCD camera to collect the re-emitted fluorescence. In their development work on fluorescent contrast agents discussed below, Achilefu and coworkers [10–13], Bugaj and coworkers [14], Zaheer et al. [15], and Becker et al. [16], employed CW techniques with area illumination and collection in their studies of targeting dye-peptide conjugates. Owing to factors such as non-uniformity of the illuminating expanded excitation beam and the inhomogeneity of endogenous absorption and scattering properties of animal tissues, direct and accurate quantitation of targeting dye accumulation within tissues was not possible. Tomographic reconstruction of dye concentration also is not possible from these studies, as described further in the next section. Nonetheless, qualitative assessment of the targeting capacity of developed dye-peptide conjugates was made possible. Area illumination and area detection has proven useful and valuable for small-animal imaging for development of NIR fluorophores.

In studies of spontaneous canine mammary disease probed with area illumination using an expanded and intensity-modulated excitation beam and area collection of the intensity-modulated emission light, Reynolds et al. [17] and Gurfinkel et al. [18] followed the accumulation of non-specific and specific dyes in the mammary chain and within regional lymph nodes. Upon collecting the amplitude of the detected modulated fluorescent signal, the ambient non-modulated light was rejected from the measurement, enabling data collection under less than dark-room conditions. The images of detected amplitude, average of detected amplitude, and phase delay across the surface of the illuminated tissue further showed the ability to localize sub-surface lesions and regional lymph nodes as deep as 1–3 cm. Owing to sub-second integration times afforded by the use of a gain-modulated intensified CCD camera [19,20], the calculation of the kinetics of dye accumulation were enabled from the sequential images, providing indication of the specificity of the dyes employed. To date, the tomographic reconstruction of fluorescence from area illumination and area collection has not been presented in the literature. In addition, while time-dependent measurements such as TDPM and FDPM measurements enable tomographic recovery of fluorescence decay parameter maps [21], to date recovery from experimental measurements has not been demonstrated.

1.3. NIR fluorescence-enhanced optical tomography

The process of tomography involves conducting measurements of the re-emitted excitation and emission light from the boundaries of tissue, using a mathematical model describing light propagation and fluorescence generation, and finally reconstructing the

interior optical properties to delineate disease. To date, researchers conducting studies on optical tomography have employed the diffusion model of light propagation, which requires that the detected signals be randomized in their direction and that only multiple scattered light is collected (for review see references [8,22,23]). As a general rule of thumb, light that has been scattered and collected after it has traveled at least 10 times the mean-free scattering length can be considered to be multiply scattered. Most biological applications in which the mean free-scattering length is on the order of millimeters require that measurements be conducted between points of incident illumination and collection that are separated by at least one centimeter. Consequently, the tomographic reconstruction of optical images from small-rodent models using the diffusion approximation may be questionable, and more appropriate methods using the full radiative transfer equation as pioneered by Hielschler et al. [24] are required. Therefore, tomographic reconstruction of fluorescence-enhanced imaging using small animals is not directly translatable to the clinically relevant volumes because the physics of light propagation differ and prevent a convenient "scale up" methodology.

Nonetheless, there have been several experimental demonstrations of tomographic reconstruction of absorptive cross section owing to fluorophore. Ntziachristos and coworkers demonstrated NIR fluorescence-enhanced tomography from CW measurements in a mouse model with targeting and reporting agents [25]. The study involved CW measurements between circumferential points of excitation illumination and fluorescence collection around a 74-cm^3 cylinder containing a mouse and index-matching fluid. In contrast, using FDPM measurements, Lee and Sevick-Muraca [26] and Hawrysz et al. [27] conducted transmittance and reflectance measurements across a 260-cm^3 tissue-mimicking phantom using point illumination of excitation light and point collection of fluorescence to reconstruct images of heterogeneities. More recently, this work has been extended using unique Bayesian tomographic algorithms [28] to hemispherical phantoms of approximately 1000-cm^3 volume [29]. The most clinically relevant application of area excitation illumination and area fluorescence detection over a wide field of view has not been the subject of tomographic algorithm development to date but was demonstrated experimentally by Roy [30]. The translation of NIR fluorescence-enhanced optical imaging requires the continued tomographic algorithm development in geometries that are pertinent to clinical imaging.

2. Limitations to fluorescent-enhanced optical imaging and tomography

In contrast to nuclear and small-animal bioluminescence imaging, fluorescence-enhanced imaging requires incident illumination with excitation light to recover an NIR fluorescent signal at the tissue surface. Frequently, the fluorescence signals emitted at a particular location on the tissue surface can be several orders of magnitude smaller than are the excitation signals emitted from the same location and comparable to the ambient light under non-dark-room conditions. In the latter case, the FDPM system of discriminating signals that are modulated at MHz modulation frequencies enabled reduction in the noise floor for fluorescent signals [7]. The former case is more problematic. Unfortunately, discrimination of fluorescent from excitation light signals often is accomplished via optical filters whose excitation light rejection capabilities are insufficient for resolving the fluorescent signals from small quantities of dye. Whether FDPM or CW measurements are employed, the limitation owing to excitation light leakage limits the noise floor of the measurements. For clinical translation, the excitation rejection capabilities must be improved to image nanomolar to picomolar concentrations of fluorescence contrast agents at significant tissue depths.

A limitation that has been overcome in tomographic work using point illumination and point collection geometries, but not yet addressed in the literature for area illumination and area collection, is the spatial variation of the incident excitation source power [26,31]. This is problematic especially for whole-body expanded beam illumination of excitation light for recovery of fluorescence using CCD detection. Using a series of polarizers to segregate the specularly reflected component of excitation light from the diffuse portion, Thompson et al. showed that one can characterize the spatial variation of an incident excitation light [32]. The work shows that, on properly characterizing the spatial variation of the incident excitation light illuminating the surface of a tissue-mimicking phantom, diffusion model-based prediction of the generated fluorescence can match that measured experimentally using FDPM techniques. This work paves the way for model-based image reconstruction from area detection of fluorescence signals resulting from area illumination of excitation light [30].

One approach to circumventing spatial variation in excitation power, heterogeneity of tissue chromophores, and variation in noise floor in small-animal

imaging is to conduct rapid measurements (whether CW measurements or amplitude measurements in FDPM) to follow temporal change in fluorescent intensity, from which pharmacokinetic parameters can be recovered. Assuming that the spatial distribution of excitation light and that tissue endogenous absorption remains constant in time during the imaging procedure, the map of pharmacokinetic parameters provides an indication of specificity for the fluorescent contrast agent in small-animal studies. This contribution provides an illustration of the usefulness of pharmacokinetics in studying a peptide-targeting paradigm directed to the epidermal growth factor receptor (EGFR) that is overexpressed in some cancers.

Before presenting this work, the following section reviews the current status and development of fluorescent contrast agents for molecular targeting of disease using fluorescence- enhanced optical imaging approaches.

3. Current research in fluorescent dye development

Characteristics important to consider in optimizing imaging properties of NIR dyes include the following: (1) the fluorophore should possess an excitation/emission spectra with maxima in the NIR wavelengths (700–900 nm) to allow for minimal absorption by endogenous chromophores such as hemoglobin, lipids, and water; (2) the fluorophore should possess a high quantum yield; (3) the fluorophore should be stable chemically and optically; and (4) the fluorophore should exhibit suitable pharmacological properties, including a high specificity for the desired target and few non-specific interactions. Over the last several years, NIR fluorophores with optimal photochemical properties have been developed.

3.1. Indocyanine green

Of the heptamethine NIR fluorophores, the indolyl (indo)cyanines show particular promise. Indocyanine green dye (ICG) (Structure A, Figure 1) and its derivatives remain the best candidates due to favorable excitation and emission at 805 nm and 835 nm, respectively, which occur at wavelengths where blood and tissue are relatively transparent. Clinical use of ICG was approved as early as 1956 (IC-Green^{TM}, Akorn, Inc., Buffalo Grove, IL). The dye has maintained a remarkably good safety profile since its introduction into clinics. ICG provides optimal imaging of choroidal circulation, making it an excellent adjunct to fluorescein angiography. ICG also has been used clinically for monitoring cardiac output and for assessing hepatic function [33,34]. Furthermore, ICG is highly bound to plasma protein as compared with fluorescein dye (98% versus 45%) and, as a result, does not leak from vessels as readily (http://www.Akorn.com). Consequently, it is used primarily as a blood-pool agent for NIR imaging.

In addition to its non-specificity, ICG undergoes a well-documented aggregation process in aqueous media, resulting in a wavelength shift of the main absorbance peak and a concurrent loss of absorption and fluorescence [35]. Therefore, there exists a need for a novel composition that improves the dye stability in solution, is simple to prepare, and, most importantly, retains the high fluorescence yield *in vivo*. Rajagopalan et al. reported non-covalent interaction of an anionic polymer, sodium polyaspartate, with ICG that produced an enhanced fluorescent stability of the dye in aqueous solution [36]. When left in aqueous solution and kept in clear bottles under normal laboratory lighting conditions, ICG lost most of its fluorescence due to aggregation. However, mixture of ICG with polyaspartate resulted in a solution that retained strong fluorescence even at day 24 under the same storage conditions [36].

Others have attempted to devise analogs of ICG with improved physiochemical properties, and more importantly, to obtain NIR dyes with functional groups that can be used readily to label biomolecules such as peptides, proteins, drugs, and oligonucleotides.

3.2. Other fluorescent labeling agents for conjugation

Ito et al. reported the synthesis of ICG succinimidyl ester (ICG-OSu) as an NIR-labeling dye in which one of the sulfonyl groups in ICG was replaced by a carboxyl group (Structure B, Fig. 1) [37]. The method was later extended to the preparation of ICG-acyl-1,3-thiazolidine-2-thione (ICG-ATT) (Structure C, Fig. 1) for the selective labeling of amines [38]. ATT reacted efficiently with amine but not with hydroxyl and sulfhydryl groups. Unfortunately, these dyes suffer poor water solubility [38]. Even after an additional sulfonate was introduced through the use of N-dydroxysulfosuccinimide, the ICG-sulfo-OSu dye still was not soluble enough to dissolve in water. In the labeling reaction, ICG-sulfo-OSu was added to the buffer solution of protein as DMSO solution [37]. As expected of highly liposoluble ICG dyes, proteins labeled with ICG were not stable in phosphate-buffered saline (PBS) solution due to dye-dye interaction and ag-

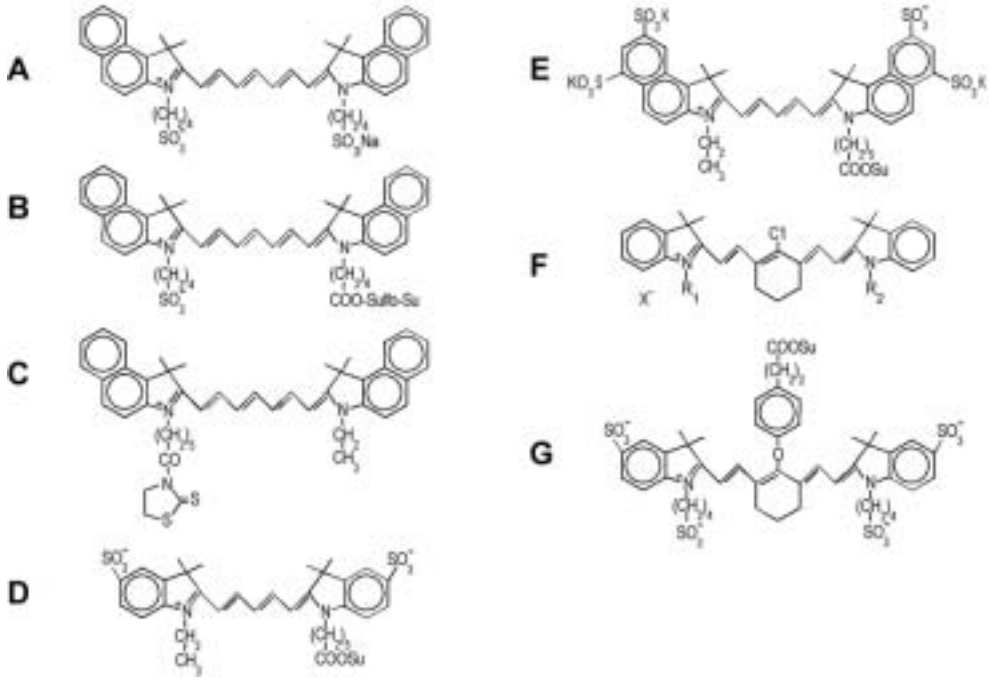

Fig. 1. Structures of various fluorescent contrast agents employed in NIR optical imaging studies. A. ICG; B. ICG-Sulfo-Osu [37]; C. ICG-ATT [38]; D. Cy5 [39]; E. Cy5.5 [40]; F. Heptamethine Cyanine Dye [41]; G. IRDye78 [42].

gregation. Furthermore, dye-dye interactions at high-labeling densities led generally to fluorescence quenching, limiting the brightness with labeled proteins and loss of absorption over time [37].

CyDye fluors (Amersham Biosciences, Piscataway, NJ) are one of the popular choices for NIR fluorescent labeling. Mujumdar et al. initially reported the synthesis of amino-reactive cyanine dyes that contain a negatively charged sulfonate group on the aromatic nucleus of the indocyanine fluorophore [39]. These sulfoindocyanine dyes are highly water-soluble and can be used to prepare brightly fluorescent materials that show low non-specific binding. Furthermore, the wavelengths of cyanine dyes can be tuned by altering the heterocyclic nucleus and the number of double bonds in the polymethine chain. Building upon their original synthesis of cyanine dyes from indocyanine heterocyclic nuclei [39], Mujumdar et al. introduced sulfonate groups at various positions on the benzindocyanine dye with the promise that benzindocyanine can shift the absorbance 30 nm toward longer wavelengths than the corresponding indocyanine dye [40]. It was noted further that, to prevent dye-dye aggregation with associated fluorescence quenching, it was necessary to introduce two sulfonate groups on each of the benzindolenine nuclei. The structures of Cy5 dye based on indocyanine heterocyclic nucleus and Cy5.5 dye based on benzindocyanine heterocyclic nucleus are shown in Fig. 1 (Structure D & E).

Narayanan and Patonay reported a simple synthetic procedure for heptamethine cyanine dyes through the use of 2-chloro-1-formyl-3-(hydroxymethylene) cyclohex-1-ene as an unsaturated bisaldehyde [41]. An important feature of this method is that asymmetric dyes derived from two different heterocycles may be synthesized in a single pot due to better control of the reaction rate. Another feature is that, in addition to the activated alkyl side chain, the vinylic chlorine on the cyclohexene bridgehead of the dye can be displaced by nucleophilic substitution to introduce amine-reactive functional groups (Structure F, Fig. 1) [41,42]. Compared to CyDye fluors, a major limitation of these dyes is the lack of water solubility required to avoid dye-dye interaction and non-specific binding. To increase aqueous solubility of this series of heptamethine indocyanine dyes, polysulfonate groups were introduced to both alkyl chains and indocyanine heterocycles [43]. The resulting dye, termed IRDye78, now is available commercially (LI-COR, Lincoln, NE) as an N-hydroxysuccinimide ester of 3-(p-hydroxyphenyl) propanoic acid substituted on the cyclohexene bridgehead of the dye (Structure G, Fig. 1). Note that nu-

cleophilic attack can occur at the cyclohexene bridgehead, resulting in the displacement of the fluorophore from the phenoxylpropionic acid group and the protein molecule attached to it, essentially decoupling the fluorophore and ligand [43].

3.3. Targeting fluorescent probes

To achieve receptor localization and specific imaging of cancer, fluorescent dyes have been attached to various ligands. The benefit to such specific targeting schemes is clear: the high selectivity and affinity of receptor ligands result in a high signal-to-noise ratio and also enable the use of low (picomolar to nanomolar) concentrations of the compounds [16]. Most of the published fluorescent probe studies are targeted at cancers (at the tumor cells themselves, or at molecular markers of the disease) to identify malignant lesions, for defining tumor spread to adjacent tissues, and as a guide for optimizing treatments of solid tumors.

3.3.1. Tumor targeting dye-antibody conjugates

Targeting fluorescent dyes for optical imaging was first attempted by the direct conjugation of cyanine dyes to monoclonal antibodies that are directed against certain tumor-associated antigens [44–46]. Folli et al. showed specific tumor targeting first using an anti-carcinoembryonic antigen monoclonal antibody coupled with fluorescein (anti-CEA mAb-fluorescein) [44] and later using the monoclonal antibody E48 coupled to indopentamethinecyanin (mAb E48-indocyanin) to target squamous cell carcinomas in mice [45]. The studies reported tumor localization by both conjugates with tumor-to-normal tissue ratios of 10 and 8 for the case of the mAb-fluorescein conjugate and the mAb-indocyanin conjugate, respectively. Furthermore, the mAb-indocyanin conjugate resulted in a clearly detectable fluorescent signature due to its excitation and emission wavelengths at 640 nm and 667 nm, respectively; whereas the fluorescence from mAb E48-fluorescein was detected only after removal of the mouse skin due to fluorescein's emission at lower wavelengths ($\sim$500 nm) [45]. These results further demonstrate that the efficiency of tumor immunophotodiagnosis can be improved by coupling to fluorochromes absorbing and emitting in the red or infrared wavelengths.

Ballou et al. prepared fluorophore conjugates of the cyanine dyes Cy3, Cy5, and Cy5.5 and two well-understood tumor-targeting antibodies; namely, anti-SSEA-1, which localizes tumors that express the SSEA-1 antigen, and antibody 9.2.27, which is directed to a human melanoma antigen [46]. Compared to fluorescein, these dyes exhibit more favorable fluorescent signatures, emitting in the red wavelengths (emission maxima for Cy3, Cy5, and Cy5.5 occur at 575 nm, 675 nm, and 700 nm, respectively). In their studies, mice were tail-vein injected with 10–100 μg of the fluorophore-antibody conjugates and imaged using either a cooled CCD or intensified video camera. The resulting fluorescence images demonstrated that, although Cy3-antibody conjugates targeted tumors, the Cy5 and Cy5.5 conjugates were more effective in visualizing the tumors, particularly in deeper tissue, again due to their fluorescence at longer wavelengths. The studies also showed that the conjugate-tumor interaction was so effective that fluorescence still was visualized from the tumor tissue five days after injection.

Additionally, it is well known that EGFR is overexpressed in many types of cancer. Soukos et al. report the use of an anti-EGFR monoclonal antibody to target a diagnostic fluorescent dye, Cy5.5, and a photochemically active dye, chlorin$_{e6}$, for photodynamic therapy in the hamster cheek pouch carcinogenesis model [47]. Using a CCD camera and simple CW fluorescence imaging, they observed specific targeting of the antibody-Cy5.5 conjugate and noted that the best contrast between normal and carcinogen-treated cheek pouches occurred between four and eight days after injection [47]. Using the antibody-chlorin$_{e6}$ construct, they were able to specifically target tumor cells and subsequently perform photodynamic therapy to reduce the size of the tumors. The results demonstrate the potential for development of immunophotodiagnosis as both a diagnostic tool and a method for monitoring response to photodynamic therapy. Together, these works gave credence to and set the stage for the burgeoning field of molecular-based optical imaging for disease diagnosis.

3.3.2. Tumor targeting dye-peptide conjugates

Although dye-antibody conjugates were a major breakthrough in the field of optical imaging, several unfavorable features were inherent in the approach. Large biomolecules, such as antibodies, often would elicit an adverse immunogenic reaction [48]. The long plasma half-life of the antibodies also would result in high background fluorescence and long blood clearance times [12,48]. Additionally, the biomolecules often are taken up preferentially by the liver [10]. Finally, for the detection of solid tumors that require the diffusion of contrast agents from the vasculature, the penetration of large dye conjugates is unfavorable due to the net positive pressure within the tumor [49]. As a result,

researchers recently devised a viable alternative to the dye-antibody conjugate. In this paradigm, the fluorescent dye is attached to a small bioactive peptide that specifically targets over-expressed tumor receptors.

Making use of a simple CW optical imaging system for *in vivo* fluorescence detection in a rat model, Achilefu et al. and Bugaj et al. studied peptide conjugates of the dye cypate, an ICG analogue [10,12,14]. They demonstrated that the cypate dye-octreotate peptide conjugates, designated cytate-1 and cytate-66, specifically target somatostatin receptor-rich tumors and specifically bind to the sst_2 receptors through the octreotate peptide [10,12,14]. Furthermore, they demonstrated that the cypate dye-bombesin peptide conjugates, designated cybesin-1 and cybesin-66, selectively target bombesin receptor-rich tumors [10,12,14]. In a separate analysis, Becker et al. used an intensified CCD camera to perform *in vivo* imaging of mouse xenografts after injecting the cyanine dye-peptide conjugate indotricarbocyanine (ITTC)-octreotate. The study yielded similar high-tumor specificity for the dye-peptide conjugate, with a tumor fluorescence threefold higher than that of normal tissue up to 24 hours after injection [16].

In our ongoing work, detailed in the following section, we investigate the dye conjugate Cy5.5 bound to epidermal growth factor (EGF; Cy5.5-EGF) for imaging human breast cancer xenografts in nude mice. The results suggest that, in addition to the fluorescence contrast to differentiate tumor margins, monitoring the time course of a dye's uptake enables pharmacokinetic modeling that, in turn, can be used to delineate tumor from normal tissue when a specific contrast agent is employed.

Methodologies that employ protein-dye conjugates to target cell-surface receptors also have been investigated. Becker et al. investigated the use of macromolecules as carriers of a fluorescent contrast agent for the optical imaging of human colon cancer xenografts in nude mice [50]. In their study, they compared two protein-dye conjugates; the first consisted of an ITCC derivative covalently bound to transferrin (Tf-ITTC); the second, ITCC bound to human serum albumin (HSA-ITTC). They reported that both compounds induced increased fluorescence contrast of tumors *in vivo* due to the accumulation of the macromolecules in the solid tumors as a result of enhanced vascular permeability and ineffective lymphatic drainage of tumor interstitium. However, the Tf-ITTC conjugate induced a higher fluorescence contrast, perhaps due in part to receptor-mediated internalization of the compound in tumor cells [50].

Finally, in addition to small peptides and proteins, researchers also have investigated the use of small molecules as delivery vehicles for fluorescent dyes. Zaheer et al. reported the use of a pamidronate-IRDye78 conjugate, termed Pam78, to specifically bind hydroxyapatite, the major mineral product of osteoblasts and calcifying vascular cells [15]. In their study, a CCD camera was used to acquire *in vivo* fluorescence images following the intravenous injection of Pam78 in nude mice. In addition to demonstrating that the dye conjugate could be used to visualize most of the bony structures of the animal, they directly compared the fluorescence images with radioscintigraphy, the current gold standard for imaging hydroxyapatite. The fluorescence images provided high sensitivity, a higher resolution, and a shorter integration time (500 ms for fluorescence imaging versus 30 minutes for radioscintigraphy) [15]. Their study further demonstrates the wide scope of applications possible with NIR fluorescence imaging.

3.4. Activatable probes

Other methodologies for targeting fluorescent dyes to tumors have been proposed and investigated. Among them are schemes involving acid and enzyme cleavable conjugates of dye-biomolecules [51,52]. Weissleder et al. conjugated Cy5.5 onto a graft copolymer consisting of a poly-L-lysine backbone and methoxypolyethylene glycol side chains [51]. The dye molecules were conjugated in close proximity to each other to quench fluorescence. However, following intravenous injection into tumor-bearing nude mice, the fluorescent probe accumulated in the tumors due to its long circulation time and permeability through neovasculature. An intratumoral fluorescent signal was generated by lysosomal proteases that cleaved the macromolecule and released previously quenched fluorophore. In vivo fluorescence imaging determined a 12-fold increase in fluorescent signal and allowed for the detection of submillimeter-sized tumors [51].

Matrix metalloproteinase (MMP) activity is known to play a key role in many diseases including cancer. As a result, MMP inhibitors have been developed as anti-cancer drugs. In a recent study, Bremer et al. developed an activatable fluorescent probe for sensing MMP activity *in vivo* in tumor-bearing mice [53]. The MMP-sensitive probe consisted of quenched NIR fluorophore (Cy5.5) conjugated to an MMP peptide substrate and a graft copolymer of methoxy-polyethyleneglycol-derivatized poly-L-lysine. The probe would fluoresce when MMP enzymes cleaved the peptide sub-

strate and released previously quenched fluorophore. The fluorescent probe was injected into mice exhibiting the HT1080 human fibrosarcoma tumor model, which exhibits high MMP production. Subsequent *in vivo* imaging resulted in a significantly higher fluorescence signal from HT1080-bearing mice compared with control mice with tumors devoid of MMP activity. Furthermore, Bremer et al. demonstrated that the fluorescent probe could be used to image MMP inhibition *in vivo*. Mice with HT1080 tumors were treated with prinomastat, a potent MMP inhibitor, for two days and subsequently imaged. The images revealed that there was significantly less MMP-fluorescent signal in treated tumors compared to untreated tumors [53].

Activatable probes that do not fully quench could be imaged best with time-dependent methods of NIR imaging. Specificity of imaging could be enhanced if temporal fluorescence decay parameters were tomographically reconstructed.

3.5. Pharmacokinetics of specific and non-specific dye uptake

A means for detecting specificity of targeting probes resides in the determination of pharmacokinetics obtained directly from small-animal imaging of the spatial and temporal distribution of fluorescent signals. In previous work, we investigated the use of a modified photodynamic agent, hexylpyropheophorbide modified with carotene (HPPH-car), and monitored the pharmacokinetics of dye uptake as a means to discriminate tumor from normal tissue *in vivo* in a canine model of mammary disease [18]. Unlike the case of non-specific ICG dye, we found that pharmacokinetic parameter maps of HPPH-car were successfully able to delineate tumor from normal tissue. We reasoned that the contrast was a result of specific interactions between the carotene moiety and cell-surface low-density lipoprotein receptors commonly over-expressed on tumor cells. Furthermore, we concluded that pharmacokinetic modeling afforded a method for assessing specific dye-tumor interactions *in vivo*.

4. Example: Model for peptide targeting of EGFR as evidenced by pharmacokinetic analysis

Herein, as an example of the specificity imparted by molecularly targeting a fluorescent agent, we present results from ongoing work in which we compare the pharmacokinetics of the cyanine dye-peptide conjugate Cy5.5-EGF and the non-specific ICG to image human breast cancer xenografts in nude mice.

4.1. Fluorescent contrast agents

ICG is available commercially from Sigma (St. Louis, MO); Cy5.5 is available commercially from Amersham Biosciences (Piscataway, NJ) as a monofunctional N-hydroxysuccinimide ester. ICG was injected as a free non-specific dye, whereas Cy5.5 was conjugated to EGF (Sigma, St. Louis, MO) to target the EGFR. EGF is a 51-amino acid peptide with a molecular weight of approximately 6000 Daltons. The dye-peptide conjugate was synthesized such that there were two dye molecules per peptide. An ultraviolet/visible light spectroscopy quantification of the peptide and dye confirmed the 2:1 molar ratio. ICG was injected at a concentration of 3 μM (300 μl injection), whereas the dye-peptide conjugate was injected at a concentration of 57 μM (300 μl injection) based on dye content.

4.2. Animal model

Four- to six-week-old female athymic nude mice (nu/nu; 18–22 g) were purchased from Harlan Sprague Dawley, Inc. (Indianapolis, IN), housed five per cage, and fed by sterilized pelleted food (Harlan Sprague Dawley, Inc., Indianapolis, IN) and sterilized water. Animals were maintained in a specific pathogen-free mouse colony in the department of veterinary medicine (The University of Texas M.D. Anderson Cancer Center, Houston, TX). The facility is accredited by the American Association for Laboratory Animal Care, and all experiments were performed in accordance with the guidelines of the Institutional Animal Care and Use Committee.

MDA-MB-468 breast tumor cells that express EGFR were obtained from American Type Culture Collection (ATCC, Rockville, MD) and were cultured in DMEM/F12 supplemented with 10% fetal bovine serum (FBS). Cells were maintained at 37°C in a humidified atmosphere of 5% CO_2.

Tumor cells to be implanted into mice were harvested near confluence by incubation with 0.05% trypsin-EDTA. Cells were pelleted by centrifugation at 450 $\times$ g for five minutes and resuspended in sterile PBS. Cells (2–3 $\times$ 10^6/animal) were implanted subcutaneously into the chest region of the mice.

Prior to imaging, the mouse was anesthetized by a single dose of 50 mg kg^{-1} bw Nembutal administered via an intraperitoneal injection. A tail-vein catheter was placed for the subsequent injections of fluorescent contrast agents. Finally, the fluorescent contrast agent was injected at the time of imaging. The same mouse

was used to study both contrast agents. For each case, the injection consisted of a 0.3-ml bolus delivered via the tail-vein catheter. For the Cy5.5-EGF study, the injected dose of contrast agent consisted of 17 nanomoles of Cy5.5 (8.5 nanomoles of EGF) in saline, whereas the delivered dose of ICG was 900 picomoles in saline.

4.3. In vivo fluorescence imaging

In vivo fluorescence images of the animal were obtained every six seconds for approximately 24 minutes following injection of the contrast agent. A laser beam from a 35-mW, 660-nm (70-mW, 785-nm) laser diode served as the excitation source for the Cy5.5-EGF (ICG) experiment. The beam was expanded with a plano-convex lens to approximately 8-cm diameter such that the beam irradiated nearly the entire animal. A 660-nm (785-nm) holographic band-rejection (Kaiser Optical Systems, Inc., Ann Arbor, MI) and 710-nm (830-nm) narrow band interference (CVI Laser Corporation, Albuquerque, NM) filters combined to pass only the fluorescence originating from the Cy5.5-EGF (ICG) dye. Sufficient spectral separation exists between the excitation/emission spectra of Cy5.5-EGF and ICG to permit imaging both dyes in the same animal. The spatially preserved fluorescent light was amplified using an 18-mm Gen 3 image intensifier tube (model FS9910C, ITT Industries, Roanoke, VA). The final fluorescent images were captured using a charge-coupled device camera (model CH350, Photometrics, Tucson, AZ) with an 800-msec exposure time. Image acquisition was controlled by V++ software (Digital Optics, Auckland, New Zealand). A schematic depicting the intensified charge-coupled device (ICCD) fluorescence imaging system is presented in Fig. 2.

4.4. Data analysis

For each image, the fluorescent intensity was averaged from two equally sized regions of interest (ROI) approximately 50 mm^2 in area; one ROI encircled an area of tumor tissue and the second enclosed an area of non-tumorous normal tissue (Fig. 3). The averaged fluorescent intensity was plotted as a function of time. For the ICG experiment, the time-dependent fluorescent intensity can be described by a double-exponential four-parameter model [18]:

$$I(t) = A\exp[-\alpha t] + B\exp[-\beta t] \tag{1}$$

where

$$A = \frac{1}{\eta}\left[w_1 C_{B_0} K_t + \frac{1}{2} w_2 C_{B_0}(K - K_B)\right] + \frac{1}{2} w_2 C_{B_0} \tag{2}$$

$$B = \frac{1}{\eta}\left[-w_1 C_{B_0} K_t + \frac{1}{2} w_2 C_{B_0}(K_B - K)\right] + \frac{1}{2} w_2 C_{B_0} \tag{3}$$

$$\alpha = \frac{1}{2}(K_B + K - \eta) \tag{4}$$

$$\beta = \frac{1}{2}(K_B + K + \eta) \tag{5}$$

$$K_B = K_t + K_0 \tag{6}$$

$$\eta = \sqrt{K_B^2 - 2K_B K + K^2 + 4K_t K}. \tag{7}$$

K_t, K_o, and K represent the rate constants describing dye uptake and wash-out from the blood to tissue, from the blood to other organs such as liver and kidney, and from the tissue to the blood, respectively. C_{B_o} represents the concentration of dye in the blood at time of injection ($t = 0$), and w_1 and w_2 are weighting factors that describe the contribution to the observed fluorescent signal from dye in the tissue and dye in the blood compartments, respectively.

Similarly, the Cy5.5-EGF time-dependent fluorescent intensity can be expressed via a single-exponential three-parameter model [18]:

$$I(t) = A + B\exp[-K_B t] \tag{8}$$

where

$$A = \frac{w_1 K_t C_{B_o}}{K_B} \tag{9}$$

$$B = \left(w_2 - \frac{w_1 K_t}{K_B}\right) C_{B_o}. \tag{10}$$

For the ICG experiment, the time-dependent fluorescent intensity was fitted to Eq. (1) to obtain estimates of the pharmacokinetic parameters. Likewise, Eq. (8) was used to fit Cy5.5-EGF fluorescence intensity and obtain estimates of the respective parameters.

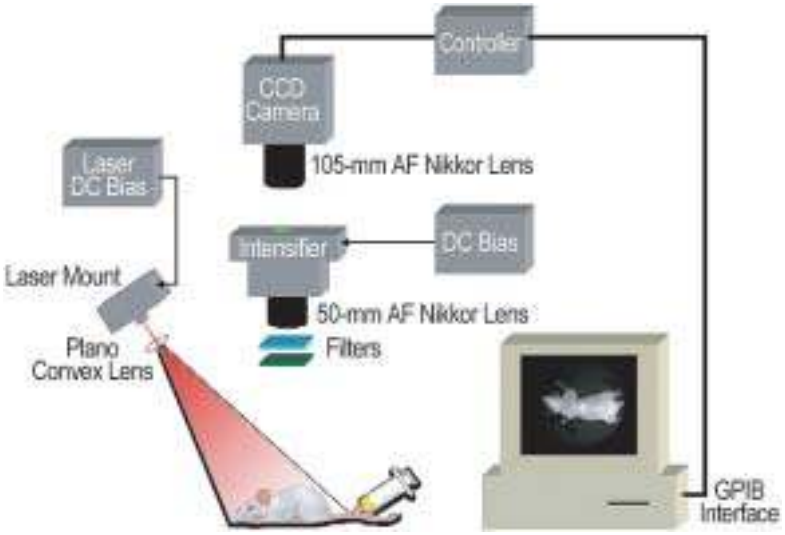

Fig. 2. Experimental system used for *in vivo* fluorescence imaging of tumor-bearing nude mice.

4.5. Results

As expected, the injection of contrast agent (ICG and Cy5.5-EGF) resulted in an immediate increase in the fluorescence signal of the whole body. Not surprisingly, in both cases the strongest fluorescent signal was observed from the region of liver. Approximately equal fluorescent signals were observed at all times post injection of ICG from the tumor-containing ROI and the ROI of normal tissue (Fig. 4). Unlike ICG, the fluorescent signal due to Cy5.5-EGF continually increased in the tumor ROI, whereas it became relatively constant in the normal tissue ROI after approximately 10 minutes (Fig. 5). Furthermore, Figs 4 and 5 show the results of the pharmacokinetic analysis on the ICG-fluorescence data and Cy5.5-EGF- fluorescence data, respectively. For the ICG-pharmacokinetic model, it is difficult to assign physical meaning to the pre-exponential parameters; however, the exponential parameters α and β conveniently sum to $K_t + K_o + K$. Furthermore, the pre-exponential parameters are signal-intensity-dependent, whereas the exponential parameters are independent of signal strength and, thus, depend only on the shape of the intensity-versus-time curve. As a result, the sum of α and β can serve as the metric by which to compare contrast based on pharmacokinetic analysis. Consequently, the sum of α and β in the tumor ROI differs by less than 15% from the value calculated in the normal ROI (calculated using Eq. (11)). This result and a qualitative inspection of the time-dependent fluorescent intensity curves for both the tumor and normal ROIs (Fig. 4) further substantiate our claim that differentiation of tumor from normal tissue based on the pharmacokinetics of ICG is futile.

Fig. 3. White light image of the mouse prior to injection of contrast agent. The highlighted squares outline the regions of interest (ROIs) used in the pharmacokinetic study. ROI 1 encloses an area of tumor tissue and ROI 2 encloses an area of normal tissue.

$$\begin{aligned}&\%\text{ change in } (\alpha+\beta) \text{ or } K_B \\ &\text{between normal and tumor tissue} \\ &\left[1 - \frac{[(\alpha+\beta) \text{ or } K_B]_{\text{tumor}}}{[(\alpha+\beta) \text{ or } K_B]_{\text{normal}}}\right] \times 100\end{aligned} = \tag{11}$$

The results of the pharmacokinetic analysis of Cy5.5-EGF data considerably differ from those for ICG. The exponential parameter K_B varies by approximately 80% between the tumor and normal ROIs (from Eq. (11)). A qualitative inspection of the time-dependent fluorescent intensity curves for the tumor and normal ROIs confirms that different mechanisms govern the observed pharmacokinetic trends. The results further corroborate the notion that pharmacokinetic analysis can be used to differentiate tumor from normal tissue when a specific contrast agent is em-

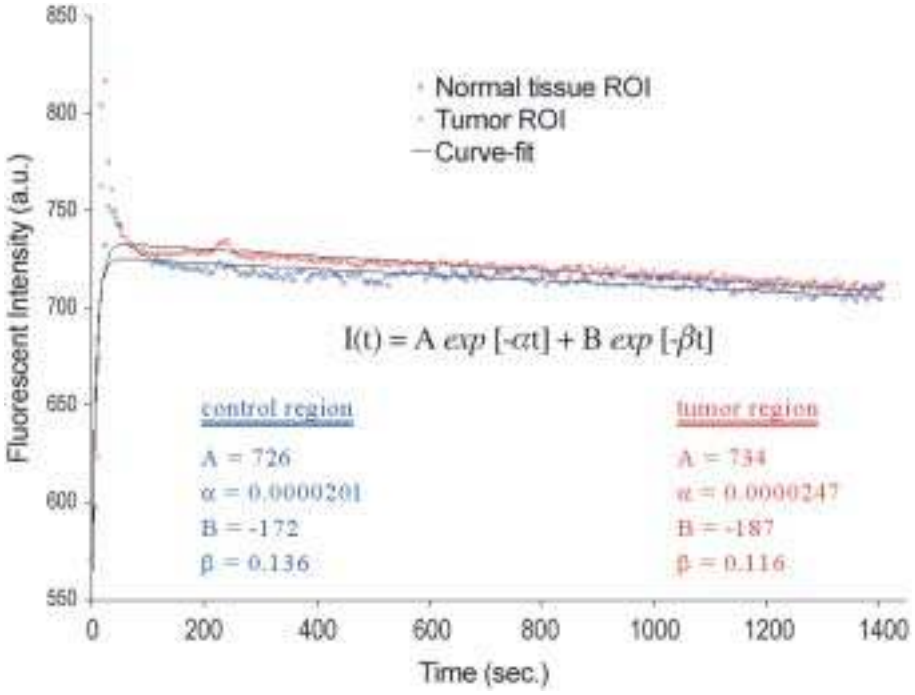

Fig. 4. Pharmacokinetics of ICG.

ployed. That is, the contrast agent must display selective and specific binding for the tumor cells.

5. Industrial and clinical applications for NIR-fluorescence-enhanced optical imaging

In the foregoing sections, we attempted to provide a balanced review of the developments and the potential for molecular imaging with NIR-fluorescent probes. To date, two distinct opportunities exist that have not been translated fully into industrial or clinical application. The first involves small-animal imaging, and the second involves diagnostic imaging in the clinic.

The opportunity for quantitative small-animal imaging using fluorescence opens significant benefits for drug discovery in evaluating the efficacy of new agents and their biodistribution. Currently, the safety and efficacy of new drugs are developed initially in studies that involve serial sacrifice of small animals to provide baseline information on toxicity, biodistribution, and bioavailability. The development of a small-animal imaging system with tomographic reconstruction of concentration of agent is imperative. To date, although there is a plethora of studies that involve small-animal imaging for fluorescent-contrast agent development, the ability for accurate tomographic reconstruction has not yet been developed adequately in the framework of proper physics. Indeed, since these small animals do not constitute significant volumes, the ability to use fluorophores that excite and emit in the visible range certainly is viable for purposes of drug discovery.

In contrast, NIR-excitable fluorescent probes are significant and required for deep-tissue diagnostic imaging in humans and possibly in the veterinary clinic. Clinical opportunities possibly may exist where diagnostic nuclear imaging techniques are employed. Certainly, gamma imaging and positron emission tomography (PET) have instrumental analogs in the measurement methods and tomography approaches outlined above for the evolving field of optical imaging. Yet, to date, owing to the lack of any approved fluorescent contrast agent for the indication of diagnostic fluorescent imaging, the feasibility of these methods remains restricted to tissue-phantoms and has yet to be validated in actual tissues.

Acknowledgements

The authors acknowledge the support of National Institutes of Health grants (R01 EB00174, R01 CA67176) and the State of Texas Advanced Technology Program.

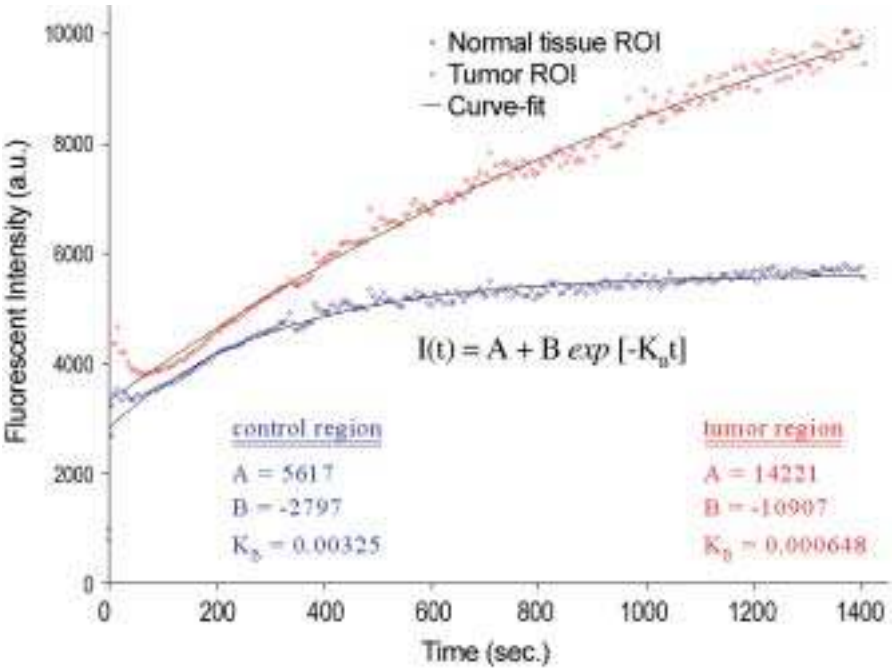

Fig. 5. Pharmacokinetics of Cy5.5-EGF.

References

[1] B.W. Pogue, S.P. Poplack, T.O. McBride, W.A. Wells, K.S. Osterman, U.L. Osterberg and K.D. Paulsen, Quantitative hemoglobin tomography with diffuse near-infrared spectroscopy: pilot results in the breast, *Radiology* **218** (2001), 261–266.

[2] E. Sevick-Muraca, G. Lopez, J.S. Reynolds, T.L. Troy and C.L. Hutchinson, Fluorescence and absorption contrast mechanisms for biomedical optical imaging using frequency-domain techniques, *Photochem Photobiol* **66** (1997), 55–64.

[3] X. Li, B. Chance and A.G. Yodh, Fluorescent heterogeneities in turbid media: limits for detection, characterization, and comparison with absorption, *Appl Opt* **37** (1998), 6833–6844.

[4] E.M. Sevick-Muraca and C.L. Burch, Origin of phosphorescence signals reemitted from tissues, *Opt Lett* **19** (1994), 1928–1930.

[5] J.R. Lakowicz, Principles of Fluorescence Spectroscopy, Plenum Press, New York, 1983.

[6] A. Chen and E.M. Sevick-Muraca, On the use of phosphorescent and fluorescent dyes for lifetime-based imaging within tissues, in: *Optical Tomography and Spectroscopy of Tissue: Theory, Instrumentation, Model and Human Studies II,* B. Chance and A.A. Alfano, eds, SPIE Press, Bellingham, WA, 1997, pp. 129–138.

[7] J.P. Houston, A.B. Thompson, M. Gurfinkel and E.M. Sevick-Muraca, Sensitivity and depth penetration of NIR fluorescence contrast enhanced imaging, *Photochem Photobiol* **77** (2003), 420–431.

[8] E.M. Sevick-Muraca, E. Kuwana, A. Godavarty, J.P. Houston, A.B. Thompson and R. Roy, Near infrared fluorescence imaging and spectroscopy in random media and tissues, in: *Biomedical Photonics Handbook,* T. Vo-Dinh, ed., CRC Press, Boca Raton, FL, 2003.

[9] T. Pan and E.M. Sevick-Muraca, Volume of pharmaceutical powders probed by frequency-domain photon migration measurements of multiply scattered light, *Anal Chem* **74** (2002), 4228–4234.

[10] S. Achilefu, R.B. Dorshow, J.E. Bugaj and R. Rajagopalan, Tumor specific fluorescent contrast agents, *Proc SPIE* **3917** (2000), 80–86.

[11] S. Achilefu, R.B. Dorshow, J.E. Bugaj and R. Rajagopalan, Novel receptor-targeted fluorescent contrast agents for *in vivo* tumor targeting, *Invest Radiol* **35** (2000), 479–485.

[12] S. Achilefu, J.E. Bugaj, R.B. Dorshow, H.N. Jimenez and R. Rajagopalan, New approach to optical imaging of tumors, *Proc SPIE* **4259** (2001), 110–114.

[13] S. Achilefu, H.N. Jimenez, R.B. Dorshow, J.E. Bugaj, E.G. Webb, R.R. Wilhelm, R. Rajagopalan, J. Johler and J.L. Erion, Synthesis, *in vitro* receptor binding, and *in vivo* evaluation of fluorescein and carbocyanine peptide-based optical contrast agents, *J Med Chem* **45** (2002), 2003–2015.

[14] J.E. Bugaj, S. Achilefu, R.B. Dorshow and R. Rajagopalan, Novel fluorescent contrast agents for optical imaging of *in vivo* tumors based on a receptor-targeted dye-peptide conjugate platform, *J Biomed Opt* **6** (2001), 122–133.

[15] A. Zaheer, R.E. Lenkinski, A. Mahmood, A.G. Jones, L.C. Cantley and J.V. Frangioni, In vivo near-infrared fluorescence imaging of osteoblastic activity, *Nat Biotechnol* **19** (2001), 1148–1154.

[16] A. Becker, C. Hessenius, K. Licha, B. Ebert, U. Sukowski, W. Semmler, B. Wiedenmann and C. Grötzinger, Receptor-targeted optical imaging of tumors with near-infrared fluorescent ligands, *Nat Biotechnol* **19** (2001), 327–331.

[17] J.S. Reynolds, T.L. Troy, R.H. Mayer, A.B. Thompson, D.J. Waters, K.K. Cornell, P.W. Snyder and E.M. Sevick-Muraca, Imaging of spontaneous canine mammary tumors using fluo-

rescent contrast agents, *Photochem Photobiol* **70** (1999), 87–94.
[18] M. Gurfinkel, A.B. Thompson, W. Ralston, T.L. Troy, A.L. Moore, T.A. Moore, J.D. Gust, D. Tatman, J.S. Reynolds, B. Muggenburg, K. Nikula, R. Pandey, R.H. Mayer, D.J. Hawrysz and E.M. Sevick-Muraca, Pharmacokinetics of ICG and HPPH-car for the detection of normal and tumor tissue using fluorescence, near-infrared reflectance imaging: a case study, *Photochem Photobiol* **72** (2000), 94–102.
[19] J.S. Reynolds, T.L. Troy and E.M. Sevick-Muraca, Multipixel techniques for frequency-domain photon migration imaging, *Biotechnol Prog* **13** (1997), 669–680.
[20] A.B. Thompson and E.M. Sevick-Muraca, NIR fluorescence contrast-enhanced imaging with ICCD homodyne detection: measurement precision and accuracy, *J Biomed Opt* **8** (2003), 111–120.
[21] E.M. Sevick-Muraca and D. Paithankar, Fluorescence imaging system and method, U.S. Patent No. 5,865,754, 1999.
[22] S.R. Arridge, Optical tomography in medical imaging, *Inverse Problems* **15** (1999), R41–R93.
[23] D.J. Hawrysz and E.M. Sevick-Muraca, Developments toward diagnostic breast cancer imaging using near-infrared optical measurements and fluorescent contrast agents, *Neoplasia* **2** (2000), 388–417.
[24] A.D. Klose, U. Netz, J. Beuthan and A.H. Hielscher, Optical tomography using time-independent equation of radiative transfer – Part 1: forward model, *J Quant Spectrosc Radiat Transf* **72**(5) (2002), 691–713.
[25] V. Ntziachristos and R. Weissleder, Experimental three-dimensional fluorescence reconstruction of diffuse media by use of a normalized Born approximation, *Opt Lett* **26** (2001), 893–895.
[26] J. Lee and E.M. Sevick-Muraca, Three-dimensional fluorescence enhanced optical tomography using referenced frequency-domain photon migration measurements at emission and excitation wavelengths, *J Opt Soc Am* **A19** (2002), 759–771.
[27] D.J. Hawrysz, M.J. Eppstein, J.W. Lee and E.M. Sevick-Muraca, Error consideration in contrast-enhanced three-dimensional optical tomography, *Opt Lett* **26** (2001), 704–706.
[28] M.J. Eppstein, D.J. Hawrysz, A. Godavarty and E.M. Sevick-Muraca, Three-dimensional, Bayesian image reconstruction from sparse and noisy data sets: near-infrared fluorescence tomography, *Proc Natl Acad Sci USA* **99** (2002), 9619–9624.
[29] A. Godavarty, M.J. Eppstein, C. Zhang, S. Theru, A.B. Thompson, M. Gurfinkel and E.M. Sevick-Muraca, Fluorescence-enhanced optical imaging in large tissue volumes using a gain-modulated ICCD camera, *Phys Med Biol* **4B** (2003), 1701–1720.
[30] R. Roy and E.M. Sevick-Muraca, Fluorescence-enhanced optical tomography with planar wave illumination, submitted to *Appl Opt* (2003).
[31] R. Roy, A. Godavarty and E.M. Sevick-Muraca, Fluorescence-enhanced optical tomography using referenced measurements of heterogeneous media, *IEEE Trans Medical Imaging* (accepted).
[32] A.B. Thompson, D.J. Hawrysz and E.M. Sevick-Muraca, Near-infrared fluorescence contrast-enhanced imaging with area illumination and area detection: the forward imaging problem, submitted to *Appl Opt* (accepted).
[33] J. Caeser, S. Shaldon, L. Chiandussi, L. Guevera and S. Sherlock, The use of indocyanine green in the measurement of hepatic blood flow and as a test of hepatic function, *Clin Sci* **21** (1961), 43–57.
[34] D.K.F. Meijer, B. Weert and G.A. Vermeer, Pharmacokinetics of biliary excretion in man VI. Indocyanine green, *Eur J Clin Pharmacol* **35** (1988), 293–303.
[35] J.F. Zhou, M.P. Chin and S.A. Schafer, Aggregation and degradation of indocyanine green, *SPIE* **2128** (1994), 495–505.
[36] R. Rajagopalan, P. Uetrecht, J.E. Bugaj, S.A. Achilefu and R.B. Dorshow, Stabilization of the optical tracer agent indocyanine green using noncovalent interactions, *Photochem Photobiol* **71** (2000), 347–350.
[37] S. Ito, N. Muguruma, Y. Kakehashi, S. Hayashi, S. Okamura, H. Shibata, T. Okahisa, M. Kanamori, S. Shibamura, K. Takesako, M. Nozawa, K. Ishida and M. Shiga, Development of fluorescence-emitting antibody labeling substance by near-infrared ray excitation, *Bioorg Med Chem Lett* **5** (1995), 2689–2694.
[38] T. Hirata, H. Kogiso, K. Morimoto, S. Miyamoto, H. Taue, S. Sano, N. Muguruma, S. Ito and Y. Nagao, Synthesis and reactivities of 3-indocyanine-green-acyl-1,3-thiazolidine-2-thione (ICG-ATT) as a new near-infrared fluorescent-labeling reagent, *Bioorg Med Chem* **6** (1998), 2179–2184.
[39] R.B. Mujumdar, L.A. Ernst, S.R. Mujumdar, C.J. Lewis and A.S. Waggoner, Cyanine dye labeling reagents: sulfoindocyanine succinimidyl esters, *Bioconjug Chem* **4** (1993), 105–111.
[40] S.R. Mujumdar, R.B. Mujumdar, C.M. Grant and A.S. Waggoner, Cyanine-labeling reagents: sulfobenzindocyanine succinimidyl esters, *Bioconjug Chem* **7** (1996), 356–362.
[41] N. Narayanan and G. Patonay, A new method for the synthesis of heptamethine cyanine dyes: synthesis of new near-infrared fluorescent labels, *J Org Chem* **60** (1995), 2391–2395.
[42] J.H. Flanagan, S.H. Khan, S. Menchen, S.A. Soper and R.P. Hammer, Functionalized tricarbocyanine dyes as near-infrared fluorescent probes for biomolecules, *Bioconjug Chem* **8** (1997), 751–756.
[43] A. Zaheer, T.E. Wheat and J.V. Frangioni, IRDye78 conjugates for near-infrared fluorescence imaging, *Molecular Imaging* **1** (2002), 354–364.
[44] S. Folli, G. Wagnieres, A. Pelegrin, J.-M. Calmes, D. Braichotte, F. Buchegger, Y. Chalandon, N. Hardman, C.H. Heusser, J.-C. Givel, G. Chapuis, A. Chatelain, H. van den Bergh and J.-P. Mach, Immunophotodiagnosis of colon carcinomas in patients injected with fluoresceinated chimeric antibodies against carcinoembryonic antigen, *Proc Natl Acad Sci USA* **89** (1992), 7973–7977.
[45] S. Folli, P. Westermann, D. Braichotte, A. Pelegrin, G. Wagnieres, H. van de Bergh and J.P. Mach, Antibody-indocyanin conjugates for immunophotodetection of human squamous cell carcinoma in nude mice, *Cancer Res* **54** (1994), 2643–2649.
[46] B. Ballou, G.W. Fisher, A.S. Waggoner, D.L. Farkas, J.M. Reiland, R. Jaffe, R.B. Mujumdar, S.R. Mujumdar and T.R. Hakala, Tumor labeling *in vivo* using cyanine-conjugated monoclonal antibodies, *Cancer Immunol Immunother* **41** (1995), 257–263.
[47] N.S. Soukos, M.R. Hamblin, S. Keel, R.L. Fabian, T.F. Deutsch and T. Hasan, Epidermal growth factor receptor-targeted immunophotodiagnosis and photoimmunotherapy of oral precancer *in vivo*, *Cancer Res* **61** (2001), 4490–4496.
[48] S.J. Goldsmith, Receptor imaging: competitive or complementary to antibody imaging? *Semin Nucl Med* **27** (1997), 85–93.
[49] R.K. Jain, Barriers to drug delivery in solid tumors, *Sci Am* **271** (1994), 58–65.
[50] A. Becker, B. Riefke, B. Ebert, U. Sukowski, H. Rinneberg, W. Semmler and K. Licha, Macromolecular con-

trast agents for optical imaging of tumors: comparison of indotricarbocyanine-labeled human serum albumin and transferrin, *Photochem Photobiol* **72** (2000), 234–241.

[51] R. Weissleder, C.-H. Tung, U. Mahmood and A. Bogdanov Jr., *In vivo* imaging of tumors with protease-activated near-infrared fluorescent probes, *Nat Biotechnol* **17** (1999), 375–378.

[52] K. Licha, A. Becker, F. Kratz and W. Semmler, New contrast agents for optical imaging: acid-cleavable conjugates of cyanine dyes with biomolecules, *Proc SPIE* **3600** (1999), 29–35.

[53] C. Bremer, C.-H. Tung and R. Weissleder, *In vivo* molecular target assessment of matrix metalloproteinase inhibition, *Nat Med* **7** (2001), 743–748.